JOURNAL OF APPLIED ELECTROCHEMISTRY **27** (1997) 1254–1264

Simulation of a polymer electrolyte fuel cell electrode

D. BEVERS, M. WÖHR

German Aerospace Research Establishment (DLR), Institute of Technical Thermodynamics, Pfaffenwaldring 38-40, 70569 Stuttgart, Germany

K. YASUDA, K. OGURO

Osaka National Research Institute (ONRI), Department of Energy and the Environment, Midorigaoka 1-8-31, Ikeda, Osaka 563, Japan

Received 14 February 1997; revised 10 April 1997

A detailed one dimensional dynamic model of a gas diffusion electrode as part of a complete fuel cell model is presented. Various effects of parameter changes are considered. Comparison of experimental results and simulation is performed and a new approach to simulation of a complete current voltage curve is discussed.

Keywords: *PEFC, simulation, gas diffusion electrode*

List of symbols

a_{act}	specific active surface ($m^2\,m^{-3}$)
b	Tafel slope (V)
c_s	heat capacity of the solid ($J\,kg^{-1}\,K^{-1}$)
$c_{p,j}$	heat capacity of component j ($J\,kg^{-1}\,K^{-1}$)
$d_{rea/diff}$	thickness of the reaction layer/diffusion layer (m)
$D_{H_2O,L}$	surface diffusion coefficient of water ($m^2\,s^{-1}$)
D_j	Knudsen diffusion coefficient of component j ($m^2\,s^{-1}$)
D_{ij}	binary diffusion coefficient between components i and j ($m^2\,s^{-1}$)
F	Faraday constant ($C\,mol^{-1}$)
ΔH_c	heat of water condensation/evaporation ($J\,mol^{-1}$)
i_{appl}	applied current density ($A\,m^{-2}$)
i_{H^+}	ionic current density ($A\,m^{-2}$)
i_o	exchange current density at open circuit potential ($A\,m^{-2}$)
j	local volumetric current ($A\,m^{-3}$)
J_j	molar flux of the component j ($mol\,m^{-2}\,s^{-1}$)
k_{eff}	effective conductivity of the electrolyte ($= \varepsilon_{el} * \kappa_{el}$) ($\Omega^{-1}\,m^{-1}$)
m	exponent of adsorption
M_j	molar weight of component j ($kg\,mol^{-1}$)
n	number of electrons involved in reaction
p	total pressure (Pa)
p_j	partial pressure of component j (Pa)
p_j^o	partial pressure of component j at reference state (Pa)
$P_{H_2O}^{sat}$	saturation partial pressure of water vapour (Pa)
r_p	pore radius (m)
R	molar gas constant ($J\,K^{-1}\,mol^{-1}$)
ΔS	reaction entropy ($J\,K^{-1}\,mol^{-1}$)
t	time (s)
T	temperature of the system (K)
U_o	open circuit potential (V)
X_s	water loading ($kg_{H_2O}\,kg_{solid}^{-1}$)
z	coordinate (m)

Greek symbols

α	cathodic charge transfer coefficient
α_v	specific surface of condensation ($m^2\,m^{-3}$)
β	material transfer coefficient ($m\,s^{-1}$)
ε_{el}	volume fraction of electrolyte
ε_g	volume fraction of pore (gas) volume
ε_g^o	volume fraction of pore (gas) volume in the water free electrode
ε_s	volume fraction of solid volume
ϕ_{el}	potential of the electrolyte (V)
ϕ_s	potential of the electric conducting material (V)
η	overpotential (V)
η_d	charge transfer overpotential (V)
η_g	dynamic gas viscosity ($kg\,m^{-1}\,s^{-1}$)
κ_{el}	conductivity of the electrolyte (bulk) ($\Omega^{-1}\,m^{-1}$)
κ_s	conductivity of the solid ($\Omega^{-1}\,m^{-1}$)
λ_s	heat transfer coefficient of the solid ($W\,m^{-1}\,K^{-1}$)
ρ_s	density of the solid ($kg\,m^{-3}$)
σ_{ij}	Lennard–Jones force constant (m)
τ_{el}	tortuosity factor of the electrolyte in the reactive layer
τ_p	tortuosity factor of the gas pores
τ_s	tortuosity factor of the solid
Ω_{ij}	collision integral

0021-891X

1. Introduction

The need for highly efficient and low emission energy conversion is directing increasing attention towards fuel cells. The polymer electrolyte fuel cell (PEFC) is considered a promising future option for vehicular propulsion [1–4] and for combined power units [5] producing both electricity and heat for low temperature purposes, for example, heating. This is due to its attainable high power density and convenience *vis-à-vis* other fuel cell types. With this increased interest in this kind of fuel cells goes an increasing wish to fully understand the governing physics in the cell and to gain ability to predict the performance of the cell under various circumstances as load, pressure and temperature based on basic parameters of the cell. Moreover, a working simulation would enable to workout further possible improvements of the fuel cell.

As part of the PEFC research programme at the Institute of Technical Thermodynamics at DLR Stuttgart [6–8] a model for a polymer electrolyte fuel cell has been developed [9–11]. As the different effects of the numerous parameters in the electrode, membrane and flow field are difficult to describe and isolate in only one paper, we will concentrate here on the fuel cell electrode which comprises a reactive layer and a diffusion layer. Since, it is generally accepted, the major difficulty in fuel cell development lies in improving cathodic performance [12–14], our focus will be on the cathode only. In the complete fuel cell model this module of the electrode is used for the oxygen side as well as for the hydrogen side with varying parameters.

2. PEFC modelling:background

Simulations of PTFE-bonded gas diffusion electrodes in a liquid electrolyte are usually based on the flooded agglomerate model [15]. Typical examples are the models of Björnholm [16] or Chan [17] for the phosphoric acid fuel cell (PAFC). For the PEFC the classical cylinder model [18] is preferred because the electrode gas transport properties can only be explained satisfactorily if there is incomplete filling of electrode pores by the solid electrolyte, especially when it is prepared from an electrolyte/catalyst paste [19–21]. Therefore, only limited transport of gases to reaction sites via the electrolyte is assumed.

The most extensive models so far have been presented by Bernardi [19] and Springer [20]. In both cases a complete model of the electrode|membrane|electrode 'sandwich' or membrane electrode assembly (MEA) has been proposed. Simulations with emphasis on the role of the membrane have been reported by Springer [12], Hill, Fales and Fuller [22–24]. Savinell [25] concentrated on the description of the anode, whereas Rho [26] gives a detailed model for the cathode. However, all the simulations mentioned above describing the electrode have in common that a satisfactory fit of experimental data could not be achieved. Large deviations between model predictions and experiment are seen, especially in the low current density region, where reaction kinetics control. Apart from Springer's model [20], the region where transport properties control is not considered or cannot be fitted to the simulation. Kim [27] fits the experimental data using a combination of an exponential and a logarithmic function, but fails to give a physical explanation of the parameters used and the parameters are changed for every curve for the same electrode.

The goal of the present work is to incorporate the known physics into a simulation, to consider the influence of changing different parameters on fuel cell performance, and to focus on the gaps and the problems that must be solved to simulate the fuel cell completely. Based on the work of Wöhr [9], a dynamic simulation of the fuel cell electrode (reactive layer and diffusion layer) has been achieved. The flow field of the bipolar plates has been purposely neglected to isolate the processes that are influenced by the properties of the electrode itself. The membrane and flow field are incorporated in the overall model of Wöhr [9]. Because it is commonly accepted that voltage losses at the anode may be neglected compared to those at the cathode [12, 13, 26], the simulation focuses on the cathode. An analysis of the anode is possible by varying certain parameters, but this is far less productive than analysis of the cathode. Solution of the differential equations has been carried out using a program package developed at the University of Stuttgart, based on the LIMEX [28] integrator. Using a modular structure, the single layers of the fuel cell, in this case the reactive layer and the diffusion layer, can be modelled and tested separately. The coupling of the modules (i.e., transfer of the boundary variables) is organized by the program package. The simulation described here is unidimensional perpendicular to the layers and has its boundaries at the interface membrane/reactive layer ($z = 0$) and diffusion layer/flow field. A scheme of the model is shown in Fig. 1.

The reactive and the diffusion layer are sandwiched between the membrane and the flow field. Both layers consist of a substrate with a certain thickness, tortuosity and porosity. The reactive layer has, in addition, a continuous electrolyte channel to the membrane inside certain pores. Nevertheless, oxygen can access reaction sites via certain pores, with no intervening electrolyte. In the simulation, it is assumed that the distribution of pore radii and tortuosities can be approximated by effective mean values in each layer.

3. Governing equations in the diffusion and reaction layer

The diffusion layer is described by the following differential equations:

Material balance of gases

$$-\frac{\varepsilon_g p_j}{RT^2}\frac{\mathrm{d}T}{\mathrm{d}t}+\frac{p_j}{RT}\frac{\mathrm{d}\varepsilon_g}{\mathrm{d}t}+\frac{\varepsilon_g}{RT}\frac{\mathrm{d}p_j}{\mathrm{d}t}=-\frac{\mathrm{d}J_j}{\mathrm{d}z} \qquad (1)$$

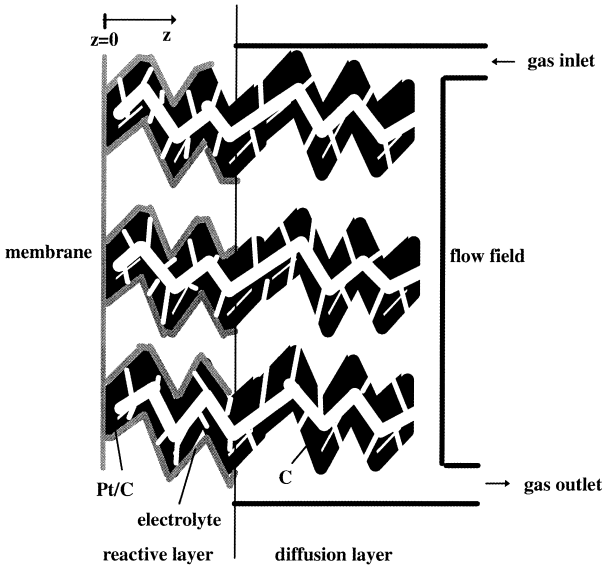

Fig. 1. Model schematic.

Material balance of water vapour

$$-\frac{\varepsilon_g p_{H_2O}}{RT^2}\frac{dT}{dt}+\frac{p_{H_2O}}{RT}\frac{d\varepsilon_g}{dt}+\frac{\varepsilon_g}{RT}\frac{dp_{H_2O}}{dt} = -\frac{dJ_{H_2O,V}}{dz}-\frac{\alpha_v\beta}{RT}\left(p_{H_2O}-p^{sat}_{H_2O}\right) \quad (2)$$

The saturation pressure of water vapour is calculated according to the Antoine equation. The pressure difference on the right side of the equation describes condensation and evaporation of water. If the water vapour pressure exceeds the temperature dependent saturation partial pressure, water will condense until the saturation pressure is reached.

However, water will evaporate (if the water loading is greater than zero) until saturation pressure is reached. If not stated otherwise, calculations are made assuming water saturated gas at all times, that is, a large evaporation surface. In view of the large surface of the carbon supports used in fuel cell electrodes and the amounts of water involved, this assumption is justified.

Material balance of liquid water

$$\frac{\rho_s}{M_{H_2O}}\frac{dX_s}{dt} = -\frac{dJ_{H_2O,L}}{dz}+\frac{\alpha_v\beta}{RT}\left(p_{H_2O}-p^{sat}_{H_2O}\right) \quad (3)$$

Energy balance

$$\rho_s c_s\frac{dT}{dt} = -\sum_{j=1}^{N}\left(J_j M_j c_{p,j}\frac{dT}{dz}\right)+\lambda_s\frac{d^2T}{dz^2} + \frac{\alpha_v\beta M_{H_2O}}{RT}\Delta H_c\left(p_{H_2O}-p^{sat}_{H_2O}\right) \quad (4)$$

In the energy balance, gas and solid phases are considered simultaneously. This assumes that gas and solid are isothermal at every base point and that the heat capacity and thermal conductivity of the gas can be neglected compared to that of the solid. Comparing the corresponding values of the media, this assumption is reasonable. It is further assumed that the thermal conductivity and heat capacity of the solid is independent of its volume fraction in the electrode. This assumption does not hold at very low volume fractions of the solid, which would also change the conductivity of the solid drastically, but it can be taken into account if necessary.

Gas transport

$$-\frac{dp_j}{dz}-p_j\frac{r_p^2}{\eta_g D_j 8}\frac{dp}{dz} = RT\left(\frac{J_j}{\frac{\varepsilon_g}{\tau_p}D_j}+\sum_{i=1,i\neq j}^{k}\frac{p_iJ_j-p_jJ_i}{p\frac{\varepsilon_g}{\tau_p}D_{ij}}\right) \quad (5)$$

$$D_j = \frac{4}{3}r_p\sqrt{\frac{2RT}{\pi M_j}}$$

$$D_{ij} = 1.8583\times10^{-3}\frac{T^{1.5}}{p\sigma_{ij}^2\Omega_{ij}}\sqrt{\frac{1}{M_i}+\frac{1}{M_j}} \quad (6)$$

The use of this equation allows simultaneous consideration of the following losses: partial pressure drop due to Stefan–Maxwell diffusion (intermolecular), Knudsen diffusion (molecule/pore–wall interaction) and Poiseuille flow caused by the total pressure gradient.

Liquid water transport

$$J_{H_2O,L} = -\frac{\rho_s}{M_{H_2O}}D_{H_2O,L}\frac{dX_s}{dz} \quad (7)$$

This equation probably represents the greatest uncertainty. There is relatively little known about water transport in heterogeneous porous systems such as the fuel cell electrode and there are different approaches to the problem. The one adopted here is to emphasize the mechanism of surface diffusion as dominant. Another possibility would have been an approach via the hydraulic pressure and the potential gradient [19]. If not stated otherwise, the simulations were performed with a large surface diffusion coefficient of water (which results in fixed porosity of the electrode) to avoid interdependencies with other parameters and misinterpretations.

Total Pressure

$$p = \sum_{j=1}^{k}p_j \quad (8)$$

Porosity

$$\varepsilon_g = \varepsilon_g^o\left[1-\left(\frac{X_s}{X_s^{max}}\right)^m\right] \quad (9)$$

$$X_s^{max} = \frac{\rho_{H_2O,L}}{\rho_s}\frac{(1-\varepsilon_s-\varepsilon_{el})}{\varepsilon_s} \quad (10)$$

$$\varepsilon_g^o = 1-\varepsilon_s-\varepsilon_{el} \quad (11)$$

In connection with Equation 7, it becomes obvious that, although water transport is a function of water loading, an increase in the latter does not result in a decrease of the effective pore radius but rather a decrease in the global value of porosity. This is a decisive assumption because water transport in fuel cells is a not well understood phenomenon. The prevailing literature opinion is that the gas is trans-

ported to the reaction sites via hydrophobic pores whereas the water is transported out of the electrode through the hydrophilic pores. Based on these assumptions, the simulation states that with increasing water loading pores are closed by the water for gas transport and vice versa. Water-filled pores therefore do not contribute to gas transport. This approach can be supported by the theory of capillary condensation which predicts a condensation in small pores beyond the actual saturation pressure [29]. For example, in pores of 10 nm diameter condensation already starts at $0.8\ P_{\mathrm{sat}}(T)$, and in smaller pores it occurs even earlier. Once all of these pores fill with water and can no longer handle water transport, larger pores will subsequently become flooded. This effect of decreasing porosity results in a diffusion hindrance of gas transport from pore flooding (via Equations 1 and 5) which will finally reduce the partial pressure of the gas.

The equations for the diffusion layer are also valid for the reactive layer after additional terms in certain equations are included to account for chemical transformation and its physico-chemical consequences.

Material balance of oxygen

$$-\frac{\varepsilon_{\mathrm{g}} p_{\mathrm{O_2}}}{RT^2}\frac{\mathrm{d}T}{\mathrm{d}t}+\frac{p_{\mathrm{O_2}}}{RT}\frac{\mathrm{d}\varepsilon_{\mathrm{g}}}{\mathrm{d}t}+\frac{\varepsilon_{\mathrm{g}}}{RT}\frac{\mathrm{d}p_{\mathrm{O_2}}}{\mathrm{d}t}=-\frac{\mathrm{d}J_{\mathrm{O_2}}}{\mathrm{d}z}-\frac{1}{nF}j \tag{12}$$

Material balance of liquid water

$$\frac{\rho_{\mathrm{s}}}{M_{\mathrm{H_2O}}}\frac{\mathrm{d}X_{\mathrm{s}}}{\mathrm{d}t}=-\frac{\mathrm{d}J_{\mathrm{H_2O,L}}}{\mathrm{d}z}+\frac{\alpha_{\mathrm{v}}\beta}{RT}\left(p_{\mathrm{H_2O}}-p^{\mathrm{sat}}_{\mathrm{H_2O}}\right)+\frac{2}{nF}j \tag{13}$$

Energy balance

$$\begin{aligned}\rho_{\mathrm{s}}c_{\mathrm{s}}\frac{\mathrm{d}T}{\mathrm{d}t}=&-\left(\sum_{j=1}^{n}J_jM_jC_{\mathrm{p},j}\frac{\mathrm{d}T}{\mathrm{d}z}\right)+\lambda_{\mathrm{s}}\frac{\mathrm{d}^2T}{\mathrm{d}z^2}\\&+\frac{\alpha_{\mathrm{v}}\beta M_{\mathrm{H_2O}}}{RT}\Delta H_{\mathrm{c}}\left(p_{\mathrm{H_2O}}-p^{\mathrm{sat}}_{\mathrm{H_2O}}\right)\\&+\left(\frac{T(-\Delta^{\mathrm{R}}S)}{nF}+\eta_{\mathrm{D}}\right)j\end{aligned} \tag{14}$$

Modelling the reactive layer requires the following additional equations:

Bulter–Volmer equation for ORR

$$\begin{aligned}j=a_{\mathrm{act}}i_{\mathrm{o}}\Bigg[&\frac{p_{\mathrm{O_2}}}{p^{\mathrm{o}}_{\mathrm{O_2}}}\exp\left(\frac{\alpha nF}{RT}\eta_{\mathrm{D}}\right)\\&-\exp\left(\frac{-1(1-\alpha)nF}{RT}\eta_{\mathrm{D}}\right)\Bigg]\end{aligned} \tag{15}$$

where $a_{\mathrm{act}}i_{\mathrm{o}}$ is the apparent exchange current density at open circuit potential. The anodic part of the equation becomes irrelevant in most cases (high overvoltage) but is included for completeness.

Ionic conduction

$$i_{\mathrm{H^+}}=-\frac{\varepsilon_{\mathrm{el}}}{\tau_{\mathrm{el}}}\kappa_{\mathrm{el}}\frac{\mathrm{d}\phi_{\mathrm{el}}}{\mathrm{d}z} \tag{16}$$

Electronic conduction

$$i_{\mathrm{H^+}}(0)-i_{\mathrm{H^+}}=-\frac{\varepsilon_{\mathrm{s}}}{\tau_{\mathrm{s}}}\kappa_{\mathrm{s}}\frac{\mathrm{d}\phi_{\mathrm{s}}}{\mathrm{d}z} \tag{17}$$

Overpotential

$$\eta_{\mathrm{D}}=U_{\mathrm{o}}+\phi_{\mathrm{el}}-\phi_{\mathrm{s}} \tag{18}$$

Volumetric current

$$-\frac{\mathrm{d}i_{\mathrm{H^+}}}{\mathrm{d}z}=j \tag{19}$$

In summary, the major assumptions for the presented simulations are:

(i) temperature of gas phase equals temperature of solid phase at every point
(ii) rapid water transport in the electrode, no flooding ($D_{\mathrm{H_2O}} \gg D_{\mathrm{H_2O,\,real}}$)
(iii) no gradient of gas concentration in the flow field
(iv) constant temperature at the boundaries
(v) rapid condensation and evaporation of water (via high specific surface of condensation; partial pressure of water vapour = saturation pressure of water in the entire cathode)
(vi) no heat storage in the gas and no heat transport through the gases by heat conduction (conductive heat transfer in gas $\ll$ conductive heat transfer in solid)
(vii) negligible change in λ_{s}, c_{s} with decreasing fraction of solid phase

Boundary conditions

for $z = 0$ (membrane)

$$T,\ J_j, J_{\mathrm{H_2O,L}}, \phi_{\mathrm{el}}, i_{\mathrm{H^+}} = i_{\mathrm{appl}},\quad \frac{\mathrm{d}\phi_{\mathrm{s}}}{\mathrm{d}z}=0$$

for $z = \mathrm{rea/diff}$ (interface reactive and diffusion layer)

$$\frac{\mathrm{d}\phi_{\mathrm{el}}}{\mathrm{d}z}=0,\quad i_{\mathrm{H^+}}=0$$

for $z = L$ (gas channel)

$$T, X_{\mathrm{s}}, p_j$$

On the one hand, the gradient of the solid phase potential, ϕ_{s}, at the membrane interface is zero as there is no electron flow into the membrane. On the other hand, the gradient of the electrolyte phase potential, ϕ_{el}, at the interface between the reactive and the diffusion layers is zero as there is no ionic current flow into the diffusion layer.

A list of the free variables of the simulation can be found in Table 1. Table 2 shows the base case parameters. If not otherwise stated, the results are the values in the stationary state.

4. Example simulations to illustrate the model

To make the following discussion more understandable and to show the potential of the simulation some general simulations will be given. These will give an idea of the quality and the quantity of the influence of major parameters (all other things being equal) on the simulation results. Stated pressures are always total

Table 1. Model variables

Reactive and diffusion layer:
$T,\ \varepsilon_g,\ X_s,\ J_{H_2},\ J_{O_2},\ J_{N_2},\ J_{H_2O_L},\ J_{H_2O_V},\ p_{H_2}, p_{O_2},\ p_{N_2},\ p_{H_2O},\ p$
Additional variables in reactive layer:
$i_{H^+},\ \eta,\ \phi_{el},\ \phi_s,\ j$
Additional variable at the boundaries:
heat flux

pressures, therefore include the partial pressure of water vapour at that temperature. The Tafel slope is kept constant in these figures ($b = 60\,\text{mV}$). It will be shown later that this assumption cannot be used to simulate a real system.

Fig. 2 shows the influence of changing the open circuit potential used to describe the electrode. It can be seen that a change of the open circuit potential simply systematically shifts the complete curve along the voltage axis. It is important to know the influence of the variation of this parameter, since the simulation assumes an ideal system. Even if all other experimental conditions remain the same, the open circuit potential in fuel cell experiments varies with the membrane electrode assembly (MEA) used. This is due to impurities on the catalytic surfaces, side reactions, differences in the effective active surface and cross-over of hydrogen and oxygen. Therefore, in simulations the open circuit potential is often used as a fitting parameter. We would like to emphasize that using a different potential than the measured open circuit potential, or the theoretical thermodynamic open circuit potential, will result in the necessity of using an apparent exchange current density which can not be verified by experiment.

Table 2. Base case parameters for the reactive and the diffusion layer

Different values for each layer are possible

Parameter	*Symbol*	*Units*	*Default* (*base*)
Surface diffusion coefficient of H_2O	$D_{H_2O,L}$	$m^2\,s^{-1}$	1.0×10^{-5}
Heat capacity of the solid	c_s	$J\,kg^{-1}\,K^{-1}$	840
Heat conductivity of the solid	λ_s	$W\,m^{-1}\,K^{-1}$	6.5
Density of the solid	ρ_s	$kg\,m^{-3}$	2000
Tortuosity factor for gas pores	τ_p	–	5
Exponent of adsorption	m	–	1
Specific condensation surface	α_v	$m^2\,m^{-3}$	1×10^9
Material transfer coefficient	β	$m\,s^{-1}$	0.001
Layer thickness (diffusion/reactive layer)	$d_{diff/rea}$	m	$170 \times 10^{-6}/60 \times 10^{-6}$
Pore radius	r_p	m	20×10^{-9}
Additional parameters in reactive layer			
Exchange current for ORR on smooth Pt surface at $b = 60\,\text{mV}$	i_o	$A\,m^{-2}$	1.0×10^{-2}
Transfer coefficient	α	–	0.6
Tortuosity factor for electrolyte	τ_{el}	–	1
Tortuosity factor for solid	τ_s	–	1
Volumetric fraction of the electrolyte	ε_{el}	–	0.2
Conductivity of the solid	κ_s	$\Omega^{-1}\,m^{-1}$	1000
Boundaries			
$z = 0$ (membrane)	$T = 80\,^\circ\text{C},\ J_j = 0,\ J_{H_2O,L} = 0,\ \phi_{el} = 0$		
$z = L$ (gas channel)	$T = 80\,^\circ\text{C},\ X_s = 0$		

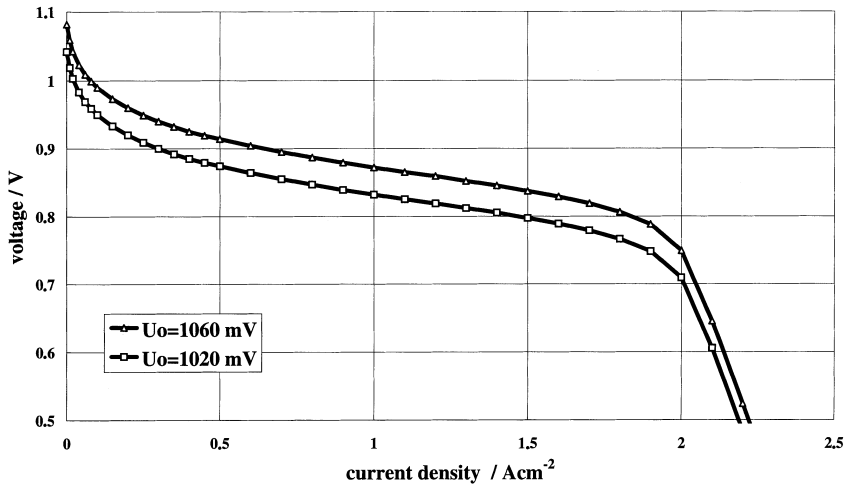

Fig. 2. Effect of a variation of the open circuit potential ($P_{O_2} = 4.87\,\text{bar},\ \varepsilon_g(\text{diff/rea}) = 12.5\%/2.5\%,\ r_{p,\,diff/rea} = 20\,\text{nm}/20\,\text{nm}$, $d_{diff/rea} = 170\,\mu\text{m}/60\,\mu\text{m},\ a_{act} = 5.9 \times 10^7, \kappa_{el} \times \varepsilon_{el} = 0.8\,\Omega^{-1}\,\text{m}^{-1}$).

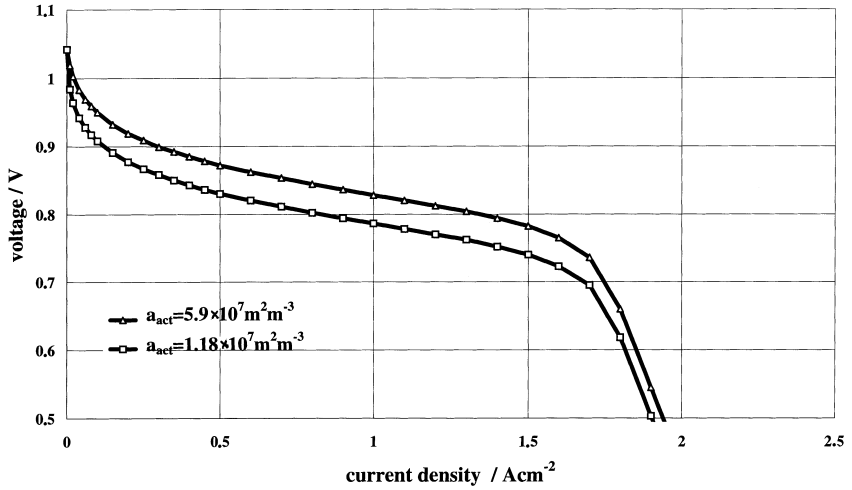

Fig. 3. Effect of a variation in the active surface ($p_{O_2} = 4.87$ bar, $\varepsilon_{g,diff/rea} = 12\%/2\%$, $r_{p,diff/rea} = 20\,nm/20\,nm$, $d_{diff/rea} = 170\,\mu m/60\,\mu m$, $\kappa_{el} \times \varepsilon_{el} = 0.8\,\Omega^{-1}\,m^{-1}$, $U_o = 1020$ mV).

The next parameter of interest is the reactive surface. It is assumed in the simulation that the actual exchange current on the platinum surface is fixed. The apparent exchange current will therefore be determined by the amount of catalytic surface per unit volume. As can be seen in Fig. 3, changing this parameter also leads to a systematic displacement of the curve at any significant current density. Only in the low current density regime does it influence the rate of the voltage drop, which is an important fact that has to be considered if this region is simulated.

The most promising approach to increase the efficiency of the electrodes in polymer electrolyte fuel cells is to incorporate solid electrolyte within the internal porous network, thereby optimizing interfacial contact and increasing reactive surface. The influence of varying the conductivity of the electrolyte within the electrode is shown in Fig. 4. As well as a similar effect as that which results from an increase in the effective reactive surface (shift of the curve at constant open circuit potential), a change in this parameter also influences the shape of the curve in the diffusion-controlled region. This effect is related to the distribution of the oxygen partial pressure and the corresponding local currents in the reactive layer, as shown in Fig. 5 and Fig. 6 for two high electrolyte conductivities (0.8 and 1.6 $\Omega^{-1}m^{-1}$; the bulk value for the Nafion 117® membrane is 10–17 $\Omega^{-1}\,m^{-1}$ [13, 19]) at current densities of 1000 mA cm^{-2} and 2200 mA cm^{-2}.

For both cases (0.8 and 1.6 $\Omega^{-1}\,m^{-1}$, Fig. 5) the pressure drop in the reactive layer for the electrode with lower electrolyte conductivity is slightly higher compared to the higher conductivity case. This is due to the different distribution of the local volumetric current, as Fig. 6 shows. The pressure drop in the diffusion layer is naturally the same for both cases, since the same amount of oxygen must be transported.

For the high proton conductivity case, current production extends more deeply into the electrode. This results in a lower local reaction rate at the reactive sites and, therefore, to a smaller overvoltage due to charge transfer resistance. Moreover, gas transport is also facilitated, so that the partial pressure drop is less. In other words, the higher the electrolyte conductivity the broader is the distribution of the reaction. If the conductivity is low, most of

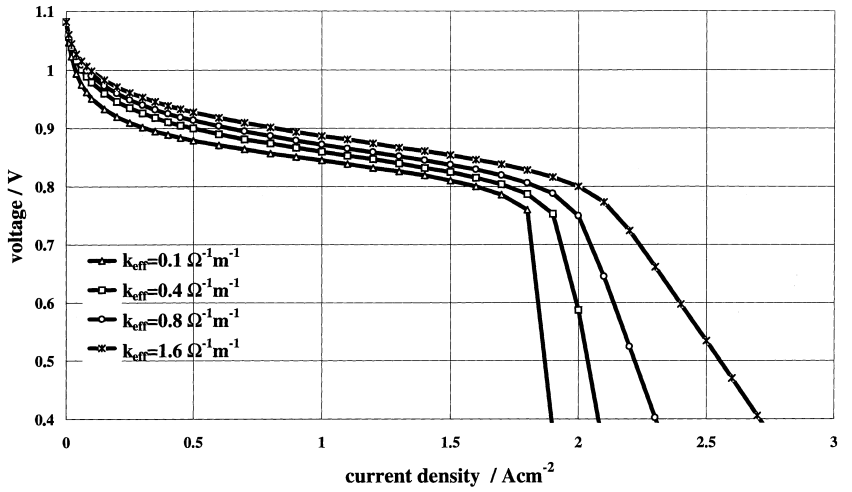

Fig. 4. Effect of a variation of the effective conductivity of the electrolyte ($P_{O_2} = 4.87$ bar, $\varepsilon_{g,diff/rea} = 12.5\%/2.5\%$, $r_{p,diff/rea} = 20\,nm/20\,nm$, $d_{diff/rea} = 170\,\mu m/60\,\mu m$, $a_{act} = 5.9 \times 10^7$, $U_o = 1060$ mV).

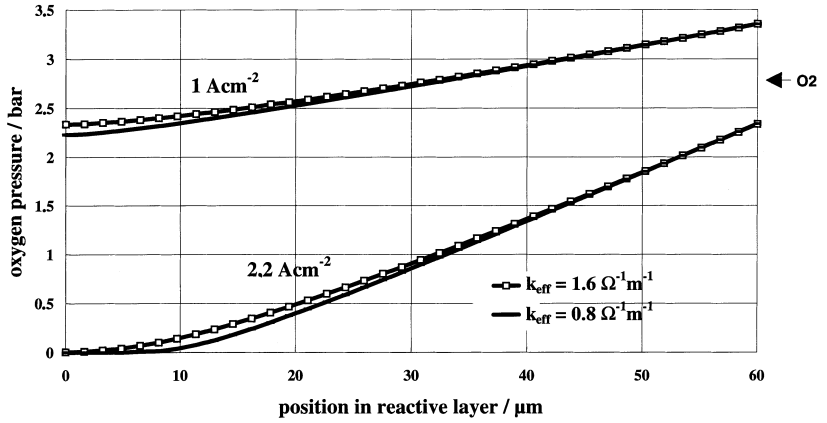

Fig. 5. Partial oxygen pressure in the reactive layer at different effective conductivities of the electrolyte and at two different current densities (data as in Fig. 4).

the reaction is restricted to the front region of the electrode contacting the membrane. Approaching the diffusion-controlled region, the electrode can only compensate the low partial pressure of oxygen by a high overvoltage and will loose potential very rapidly (see Fig. 4). For electrodes with high proton conductivity, the reaction will initially take place throughout the electrode. Approaching the diffusion-controlled area, the reaction will preferably take place closer to the gas inlet. In the case shown in Fig. 6 these effects result in a different position for the peak current production and naturally in a different absolute value of the peak in local volumetric current production:

(i) at 1 A cm^{-2}
1719 A cm^{-3} at 0.8 Ω^{-1} m^{-1} and 1016 A cm^{-3} at 1.6 Ω^{-1} m^{-1}

(ii) at 2.2 A cm^{-2}
2196 A cm^{-3} at 0.8 Ω^{-1} m^{-1} and 1134 A cm^{-3} at 1.6 Ω^{-1} m^{-1}

It should be mentioned that the effect of changing the electrolyte conductivity resembles the effect of the parameter n in Kim's model [27], where a physical interpretation was lacking.

Another parameter with a large impact on fuel cell performance is the Tafel slope b. The value of this parameter depends on the charge transfer factor α, the number of electrons transferred in the rate-determining step n and the temperature T. Fig. 7 illustrates the influence of this parameter on the current–voltage curve. The current-voltage curve drops faster over the complete range for larger b.

Finally, the influence of the pore size and the porosity of the electrode will be considered (Fig. 8). Generally speaking these two parameters determine the point of onset of diffusion control. For the case of a change of these parameters in the diffusion layer, the effect is not only a parallel movement of this region but also a change in slope. By analogy with the influence of electrolyte conductivity, the physical meaning is illustrated best by again consulting the partial pressure and local volumetric current plots.

The change in slope when changing one of these parameters in the diffusion layer is due to the resulting change in the 'input' partial pressure seen by the reactive layer. The shift in the onset of the diffusion control is due to the different location in the electrode where p_{O_2} approaches zero (Fig. 9). Beyond

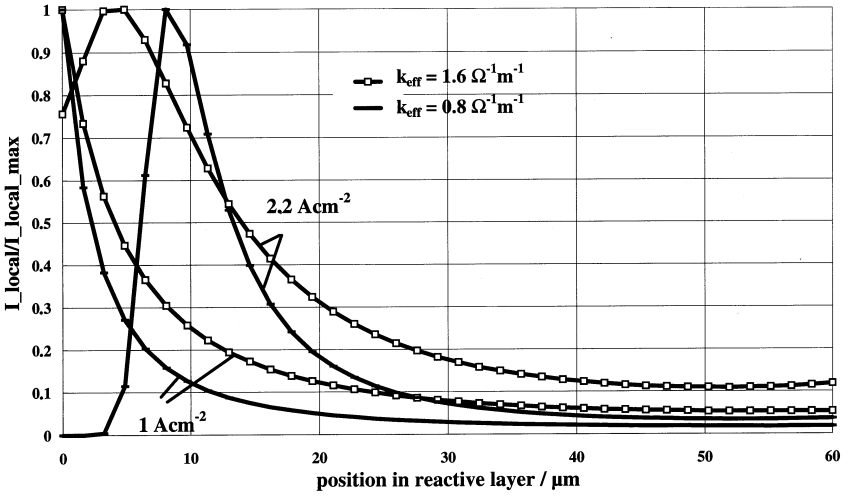

Fig. 6. Local current density in the reactive layer at different effective conductivities of the electrolyte and at two different current densities (data as in Fig. 4).

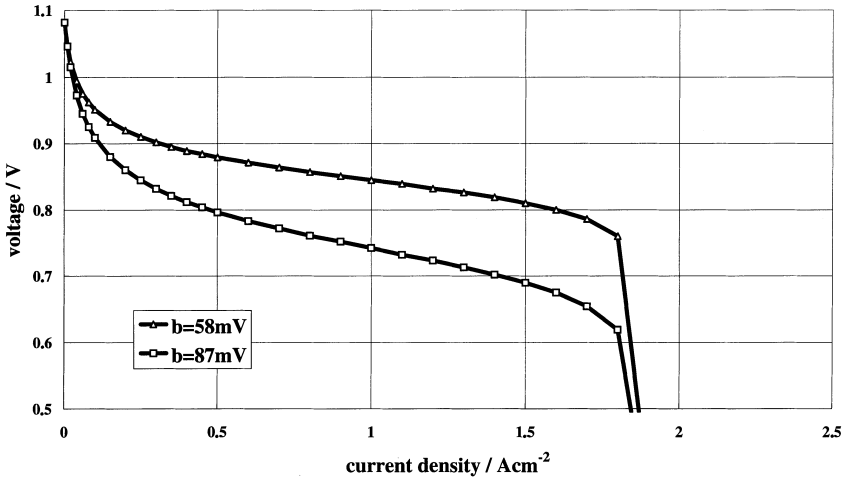

Fig. 7. Effect of a variation of the Tafel slope ($p_{O_2} = 4.87$ bar, $\varepsilon_{g,diff/rea} = 12.5\%/2.5\%$, $r_{p,diff/rea} = 20\,nm/20\,nm$, $d_{diff/rea} = 170\,\mu m\ /60\,\mu m$, $a_{act} = 5.9 \times 10^7$, $\kappa_{el} \times \varepsilon_{el} = 0.1\,\Omega^{-1}m^{-1}$, $U_o = 1060$ mV).

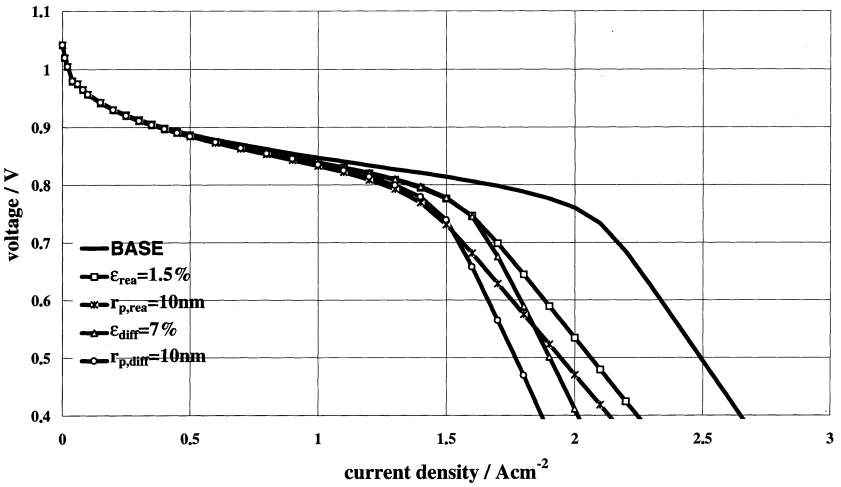

Fig. 8. Effect of a variation of the pore radius and the porosity in the reactive layer or the diffusion layer ($p_{O_2} = 4.87$ bar, base: $\varepsilon_{g,diff/rea} = 12.5\%/2.5\%$, $r_{p,diff/rea} = 20\,nm/20\,nm$, $d_{diff/rea} = 170\ \mu m/60\,\mu m$, $a_{act} = 5.9 \times 10^7$, $\kappa_{el} \times \varepsilon_{el} = 1.6\,\Omega^{-1}\,m^{-1}$, $U_o = 1020$ mV).

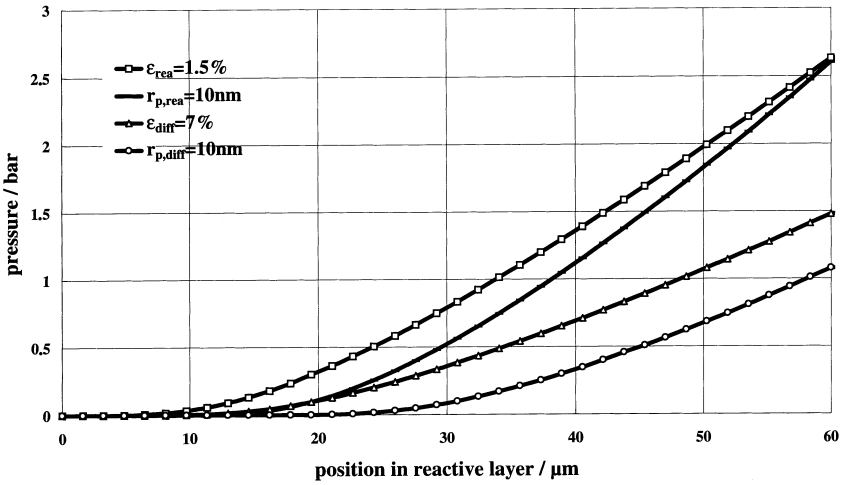

Fig. 9. Partial pressure dependence of oxygen in the reactive layer on pore radius and porosity in the reactive or the diffusion layer at $i = 1800\,mA\,cm^{-2}$ (data as in Fig. 8).

this point the low partial pressure must be compensated by large overvoltage. Before this point the influence of lower p_{O_2} is only minor because the overvoltage is in the exponent of the Butler–Volmer equation and therefore dominates numerically. The worse the electrolyte conductivity is, the greater will be the contribution of porosity and pore size in defining the onset of the diffusion control. Figure 10 shows the corresponding local volumetric current distributions.

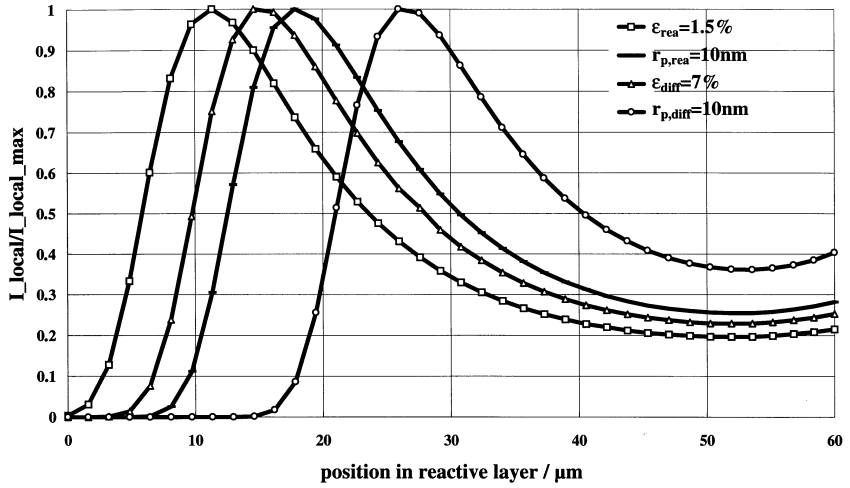

Fig. 10. Local current density dependence in the reactive layer on pore radius and porosity in the reactive or the diffusion layer at $i = 1800\,\mathrm{mA\,cm^{-2}}$ (data as in Fig. 8).

The width of the reactive area is about the same in all cases due to the fixed electrolyte conductivity. The maximum is again determined by the point of exhaustion of p_{O_2}. Moreover, a shift of the reaction to the diffusion layer side of the reactive layer can be seen for a small pore size in the diffusion layer. The influence of the layer thickness is equivalent to changing the pore diameter or the porosity, and so this is already implicit in these plots. Again, we emphasize the correspondence of the parameters determining the position of the diffusion controlled region to the empirical factor m from [27].

5. Model fit to experimental data

The main goal of this simulation was to fit a set of experimental data precisely over the complete range of observed current densities. As far as they were available, we used values for the different parameters from measurements or the literature. Nevertheless, the number of variables with no available parameters is still considerable.

Figure 11 shows a set of *IR*-drop corrected current–voltage curves as measured at ONRI (Osaka National Research Institute) with in-house-prepared electrodes [30, 31]. The only parameter changed in these measurements was the pressure. At every point an *IR*-drop was measured because of the known dependence of membrane resistance on current density [13, 32]. The parameters used for the simulation, if other than base case values, are given in the Figure legends.

The measured data were fitted for the 4.87 bar case in the low current region using a Tafel slope of 60 mV $\mathrm{dec^{-1}}$ (which is most often referred to as the Tafel slope for the oxygen reaction on platinum in this region in the literature [33–35]), using the measured open circuit potential, U_o, and varying the apparent exchange current density (by varying the active surface) until a satisfactory fit is obtained. Subsequently, the other pressures are simulated by changing the system pressure in the simulation only. The result is shown in Fig. 12.

Fitting the 4.87 bar curve results in a satisfactory fit for the other pressures up to potentials of about

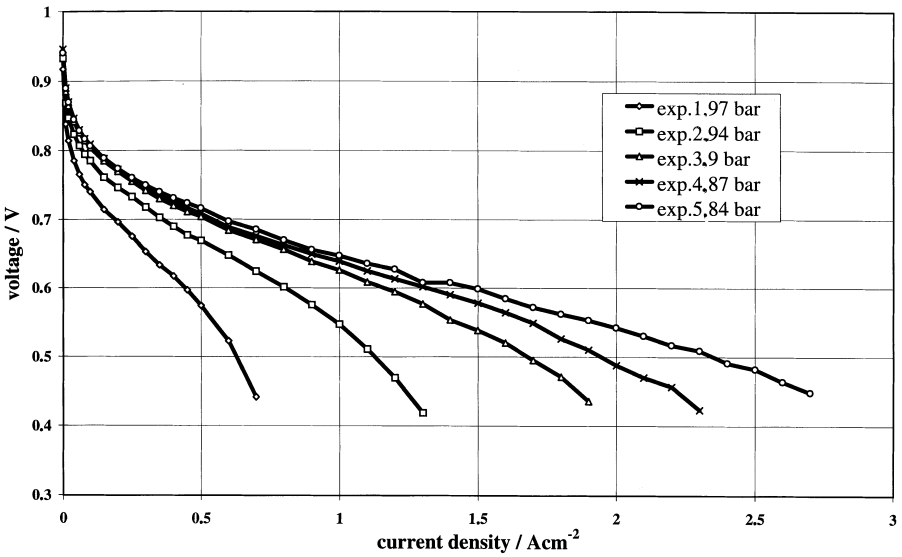

Fig. 11. Experimental data, ONRI, Nafion® 112, 90 °C, 0.1 mg $\mathrm{Pt/cm^2}$.

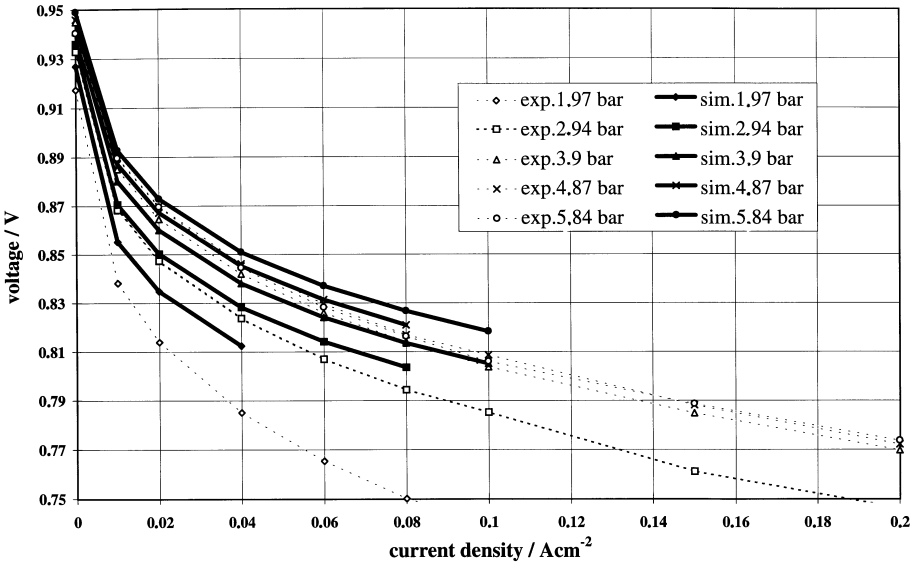

Fig. 12. Fit of the low current region of experimental data (pressures: 1.97, 2.94, 3.9, 4.87 and 5.48 bar, $\varepsilon_{g,diff/rea} = 22.5\%/2.3\%$, $r_{p,diff/rea} = 20\,nm/20\,nm$, $d_{diff/rea} = 170\,\mu m/60\,\mu m$, $b = 60\,mV$, $a_{act} = 2.3 \times 10^7$, $\kappa_{el} \times \varepsilon_{el} = 0.8\,\Omega^{-1}\,m^{-1}$, $U_o = 946\,mV$, $p^o = 4.87\,bar$).

830 mV, when the experimental curves and the simulation start to deviate. Moreover, the result for the lowest pressure deviates most from experiment. However, the likelihood is that the measured data are suspect due to the apparent insensitivity of voltage to pressure from 3.9 to 5.84 bar, suggesting some variation in electrode condition during the experiment. This is an almost unavoidable limitation in any attempt to simulate data where self-consistency is difficult to achieve. This is the case with fuel cells and does not reflect on the quality of the model itself. Differences may occur if electrochemical measurements are made starting at high pressures and going to low pressures, or vice versa. Such changes can hardly be introduced by simulation. It is, in any case, obvious that the complete curves cannot be simulated without changing the Tafel slope for the lower voltage (higher current) region. It is known [34, 35] that the reaction mechanism of the oxygen reaction on platinum changes around a potential of 800 mV. Therefore, we simulated the higher current regions by using a Tafel slope of 120 mV [34] and adopting the apparent exchange current density, i_o (indicating a change of the reaction kinetics due to a change of catalyst from Pt with adsorbed oxygen to bare Pt) until a satisfactory fit for the 4.87 bar case was achieved, but keeping all other parameters the same as those in the low current density simulation. Finally, all other pressures were calculated with the set of parameters which gave a satisfactory fit for the 4.87 bar case. The result is shown in Fig. 13.

All curves may be described with the same set of parameters. Accounting for the already mentioned obvious drift in the condition of the membrane–electrode–assembly the fit can be considered as excellent. Only in the very high current density region does the simulation give better results than the experiment. An explanation could be a gradual decrease in the active surface due to pore flooding. As seen in Fig. 3, this would result in a parallel shift of the curve towards lower voltages. This could be an indication that the porosity of an electrode should be larger than the amount necessary regarding gas diffusion alone, since product water will close some pores due to the requirements for water transport. This idea is supported by experimental results from the DLR [36] and independent work [37]. Another explanation could be the existence of higher Tafel slopes than the ones chosen resulting from temperature correction of the reported values. A real diffusion hindrance is a much more unlikely phenomenon, since the translation of the current voltage curve would then be much sharper, unless the ionic conductivity in the electrode is very high.

6. Conclusion

The simulation described here is a powerful tool for determining the influence of different parameters in an electrode on the characteristics of the PEFC. Comparison of the model with real data shows the importance of incorporating the experimental verified effect of a changing Tafel slope at about 800 mV to achieve a satisfactory fit. In addition, the simulation indicates the importance of having sufficient porosity to maintain rapid removal of product water at any practical current density. A significant outcome of the simulation is the importance of keeping the cathode potential as far as possible above the potential in which the change of the Tafel slope occurs. This can only be achieved by large values of the apparent exchange current density (excellent catalyst or large active surface). Questions remaining for further investigation concern: (i) the methodology necessary to incorporate the gradual change in Tafel slope in the simulation; (ii) a method of verification of the assumed transport mechanism of water; (iii) the real electrolyte conductivity in the electrode, and its gra-

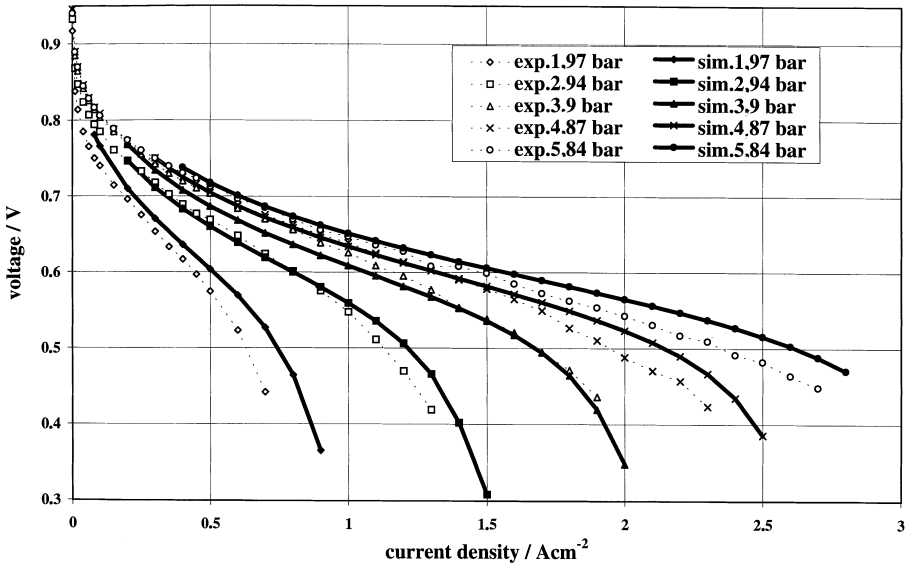

Fig. 13. Fit of complete current voltage curves (data as in Fig. 12, but $b = 120\,\mathrm{mV}$ and $i_o = 14.3 \times 10^{-2}\,\mathrm{A\,m^{-2}}$).

dient within the electrode; and (iv) a method whereby a mean pore size reflects the real case of a distribution of larger and smaller pores.

Acknowledgements

The authors gratefully acknowledge experimental support by Dr M. Mizuhata. One of the authors (D.B.) would like to thank the German Academic Exchange Service (DAAD) for making this work possible under a HSP II fellowship.

References

[1] S. Ogino and Y. Kimura, 13th International Electric Vehicle Symposium, 13–16 Oct. 1996, Osaka, Japan, p. 671.
[2] M. Iwase and S. Kawatsu, *ibid.*, p. 675.
[3] T. Moser, J. R. Rao and E. Grecksch, *ibid.*, p. 680.
[4] Daimler–Benz High Tech Report, 'Technologie 1996' pp. 14–19.
[5] M. S. Wilson, C. Zawodzinski, S. Gottesfeld and A. R. Landgrebe, Proceedings of the 11th Annual Battery Conference, Long Beach, CA, Jan. 1996, pp. 107–112.
[6] K. Bolwin, E. Gülzow, D. Bevers and W. Schnurnberger, *Solid State Ionics* **77** (1995), 324–30.
[7] D. Bevers, N. Wagner and M. von Bradke, Proceedings of the 11th World Hydrogen Energy Conference, Stuttgart, Germany, 1996, pp. 1767–76.
[8] D. Bevers, R. Rogers and M. von Bradke, *J. Power Sources*, accepted for publication.
[9] M. Wöhr, PhD thesis, University of Stuttgart, in preparation.
[10] M. Wöhr, K. Bolwin, W. Schnurnberger, W. Neubrand and G. Eigenberger, Proceedings, *op cit*. ref. [7], pp. 1861–70.
[11] M. Wöhr, S. R. Narayanan and G. Halpert, Abstracts of the 190th meeting of the Electrochemical Society, Texas, 6–11 Oct. 1996, p. 970.
[12] T. E. Springer, T. A. Zawodzinski and S. Gottesfeld, *J. Electrochem. Soc.* **138**, 1991, 2334–42.
[13] T. E. Springer, M. S. Wilson and S. Gottesfeld, *ibid.* **140**, 1993, 3513–26.
[14] Y. W. Rho, S. Srinivasan and Y. T. Kho, *ibid.* **141**, 1994, 2089–96.
[15] J. Giner and C. Hunter, *ibid.* **116**, 1969, 1124–30.
[16] P. Björnholm, *Electrochim. Acta*, **32**, 1987, 115–9.
[17] D. S. Chan and C. C. Wan, *J. Power Sources* **50**, 1994, 261–81.
[18] B. V. Tilak, R. S. Yeo and S. Srinivasan, 'Comprehensive Treatise of Electrochemistry', Vol. 3 (edited by J. O'M. Bockris, B. E. Conway, E. Yeager and R. E. White), Plenum Press, New York (1981).
[19] D. M. Bernadi and M. W. Verbrugge, *J. Electrochem. Soc.*, **139**, 1992, 2477–91.
[20] T. E. Springer, M. S. Wilson and S. Gottesfeld, *ibid.* **140**, 1993, 3513–26.
[21] K. Kawahara, T. Haga, T. Suzuki and T. Asaoka, Electric Vehicle Symposium, *op cit*. [1], pp. 713–7.
[22] R. Hill and M. Verbrugge, *J. Electrochem. Soc.*, **137**, 1990, 886–93.
[23] J. L. Fales, N. E. Vanderbrogh and P. Stroeve, The Electrochem. Society Softbound Proceedings Series, PV 86-13 (1986), p. 179.
[24] T. Fuller and J. Newman, *ibid.*, PV 89-14 (1984), p. 25.
[25] J. T. Wang and R. F. Savinell, *Electrochim. Acta*, **37**, 1992, 2737–45.
[26] Y. W. Rho, S. Srinivasan and Y. T. Kho, *J. Electrochem. Soc.*, **141**, 1994, 2089–96.
[27] J. Kim, S. Srinivasan, S. M. Lee and C. E. Chamberlin, *Proc. Electrochem. Soc.* **94-22**, 1994, 296–305.
[28] P. Deuflhard and U. Nowak, University of Heidelberg, SFB 123, Technical Report 332 (1985).
[29] W. Kast, 'Adsorption aus der Gasphase', VCH, Weinheim (1988).
[30] M. Mizuhata, K. Yasuda, K. Oguro and H. Takenaka, International Hydrogen and Clean Energy Symposium, Tokyo, Japan, 6–8 Feb. 1995, p. 309.
[31] K. Amine, M. Mizuhata, K. Oguro and H. Takenaka, *J. Chem. Soc. Faraday Trans.* **91**(24), 1995, 4451–8.
[32] T. V. Nguyen, *J. Electrochem. Soc.*, **143**, 1996, L103–L105.
[33] S. Mukerjee and S. Srinivasan, *J. Electroanal. Chem.* **357**, 1993, 201–24.
[34] A. Parthasarathy, C. R. Martin and S. Srinivasan, *J. Electrochem. Soc.* **138**, 1991, 916–21.
[35] E. Yeager, M. Razaq, D. Gervasio, A. Razaq and D. Tryk, *J. Serb. Chem. Soc.* **57**(12), 1992, 819–33.
[36] D. Bevers, PhD thesis, University of Stuttgart, in preparation.
[37] K. Kawahara, T. Haga, T. Suzuki and T. Asaoka, Electric Vehicle Symposium, *op cit*. [1] pp. 713–7.